K. HAM: HTLV-1 Associated Myelopathy（HTLV-1 関連脊髄症）

1980年HTLVが発見され，翌年にはHTLVがATLの原因ウイルスと確認された．そして，1985年6月にHAM患者第一例が発見された[22,23]．1986年11月からは，献血のHTLV-Iスクリーニング開始され，その後，スクリーニングを受けた血液由来のHAM発症はない．HAMは2008年に厚生労働省特定疾患に指定されたが，慢性進行性の疾患であり医療費軽減措置を含む総合的なHAM対策の充実が望まれる．

L. HAMの疫学

最近，HTLV-1感染者および第三次HAM患者全国調査が行われた．その結果，HTLV-1感染者は全国で約108万人存在し（図4）[24]，関東，関西などの都市圏でHAM患者が増加していることが明らかとなった（図5）[25]．また，1995年以降は高齢発症のHAM患者が多く，高齢発症割合（65歳以上）は，1994年前は4/317例（1.3％），1995年以降は122/464例（26.3％），$p < 0.0001$（Fisher's直接法）であった．ALSの有病率との比較に基づいて，HAMの人口10万人当たりの推定有病率は3.0人と推定された．

M. HAMの診断上の注意点

多発性硬化症，視神経脊髄炎，頸椎症性脊髄症などとの鑑別が重要となる．抗HTLV-I抗体価，HTLV-Iプロウイルス量，抗アクアポリン4抗体，電気生理学的検査所見が参考となる[26,27]．一般的に緩徐進行性であるが，時に急速に進行する例がある．急速進行を示すHAM患者の定義は，発症2年以内に両杖歩行レベル以上に悪化，または，

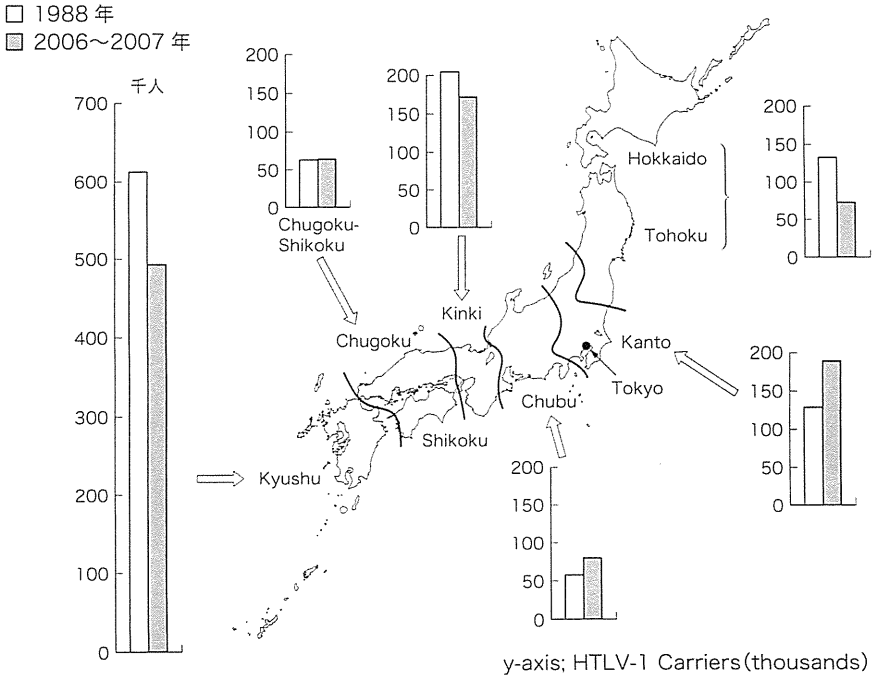

図4　HTLV-1保因者の変遷（Satake M, et al. J Med Virol. 2012; 84: 327-35）[24]
現時点のHTLV-1保因者数は108万人と推定された．

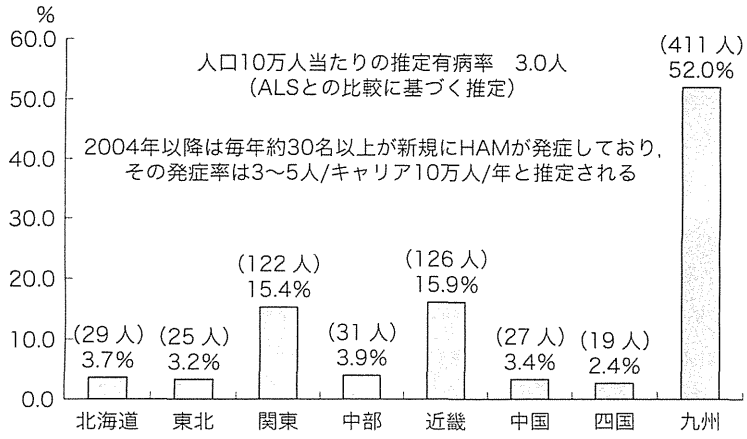

図5　第3次HAM全国調査で登録されたHAM患者790名の地域分布
(出雲周二, 他. 神経内科. 2011; 75: 369-73)[25]

3〜6カ月以内に納の運動障害重症度（OMDS）が1段階以上の悪化としている．比較的急速に症状が進行している例には，ステロイドホルモン大量投与，インターフェロンα注射（保険適応あり）などが有効な場合がある[28]．

N. HAMとリハビリテーション
–インナーマッスルの再教育–

HAMの治療において，継続的なリハビリテーション（リハビリ）は必須である．痙性のコントロールと体幹筋の再教育・強化を行うことで体幹を円筒状に強化保持し，骨盤周囲筋の再教育・強化を行うことで，足の振り出しがスムーズになりリハビリ効果の向上に役立つと考えられる（図6）[29]．ロボットスーツHAL福祉用（HAL®）はCYBERDYNE（株）により開発された装着型動作支援機器でOMDS 5度以上のHAM症例がHAL装着歩行練習に適応していると考えている．

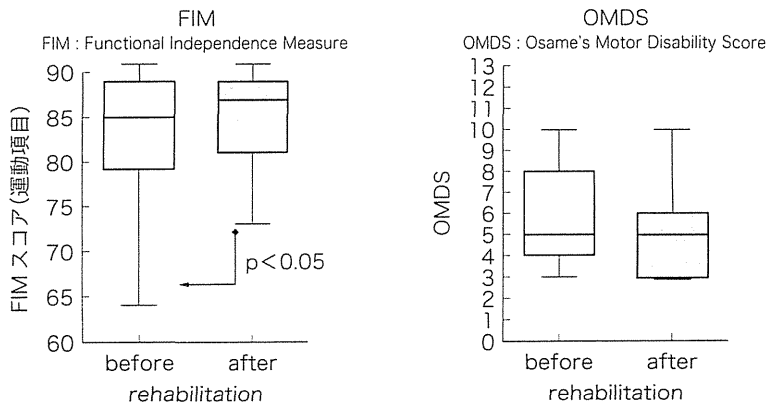

図6　HAMに対するリハビリ効果（武澤信夫, 他. 神経内科. 2011; 75: 393-401)[29]
HAM症例15例（男性3例，女性12例）に4週間の集中リハビリを行った．

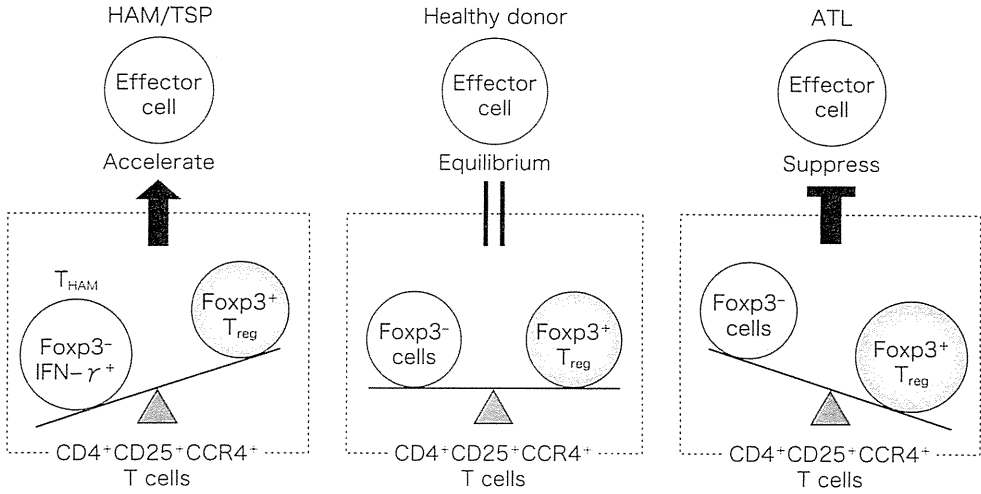

図7　HAMとATLにおける免疫反応とCD4⁺CD25⁺CCR4⁺ T細胞における T_{HAM}/T_{reg} 比
(Araya N, et al. Viruses. 2011; 3: 1532-48[37] より改変)

O. HAM患者に対するバクロフェン髄注療法(ITB療法)

バクロフェンは，脊髄後角に分布する$GABA_B$受容体にアゴニストとして作用し，γ運動ニューロンの活性を低下させる．バクロフェン髄注療法(ITB療法）が開発され，わが国でも2006年4月保険適応となった．われわれは，ITB療法のスクリーニングで有効性が認められたHAM患者3例にバクロフェン髄注療法用ポンプの埋め込み術を行い，その後，継続的なリハビリを施行した．三次元動作解析装置（VICON MX）を用いて，歩行中の計測空間に対する骨盤角度，左右の下肢の各関節角度を計測し，3例ともに下肢痙性および歩行の改善を認めた．

P. HAMの病態

脊髄の病理学的検討から，HAMでは胸髄中下部の左右対称性の側索，前側索，後索腹側部の変性，血管周囲から実質内にひろがる小円形細胞の浸潤がみられる[30-33]．HTLV-I mRNAおよびプロウイルスDNAは浸潤単核細胞内のCD4陽性Tリンパ球内にのみ確認される．HAMの発症にはホスト側とウイルス側の発症関連要因（HLA，ウイルスタイプなど）が関与している．脊髄病巣部のHTLV-1感染CD4陽性Tリンパ球とそれを攻撃するHTLV-1特異的CD8陽性Tリンパ球との相互作用により種々のサイトカインが持続的に放出され，神経組織を傷害していると想定されている（by stander効果)[34]．

Q. HAMに関連した最近の研究

HTLV-1 basic leucine zipper factor(HBZ)は，HTLV-1Tax遺伝子の逆方向からの転写により産生される．Saitoらは，HAM 56例のHBZ mRNA発現量を検討し，HAM重症度および髄液中ネオプテリン量と相関し，IFN-α治療により減少すると報告している[35]．Yamanoらは，IFN-γ⁺CD4⁺CD25⁺CCR4⁺T細胞（T_{HAM}）がHAM患者で増加しており，HAMの臨床的重症度および髄液中ネオプテリン量と相関していると報告している（図7)[36,37]．Satouらは，HAM患者では

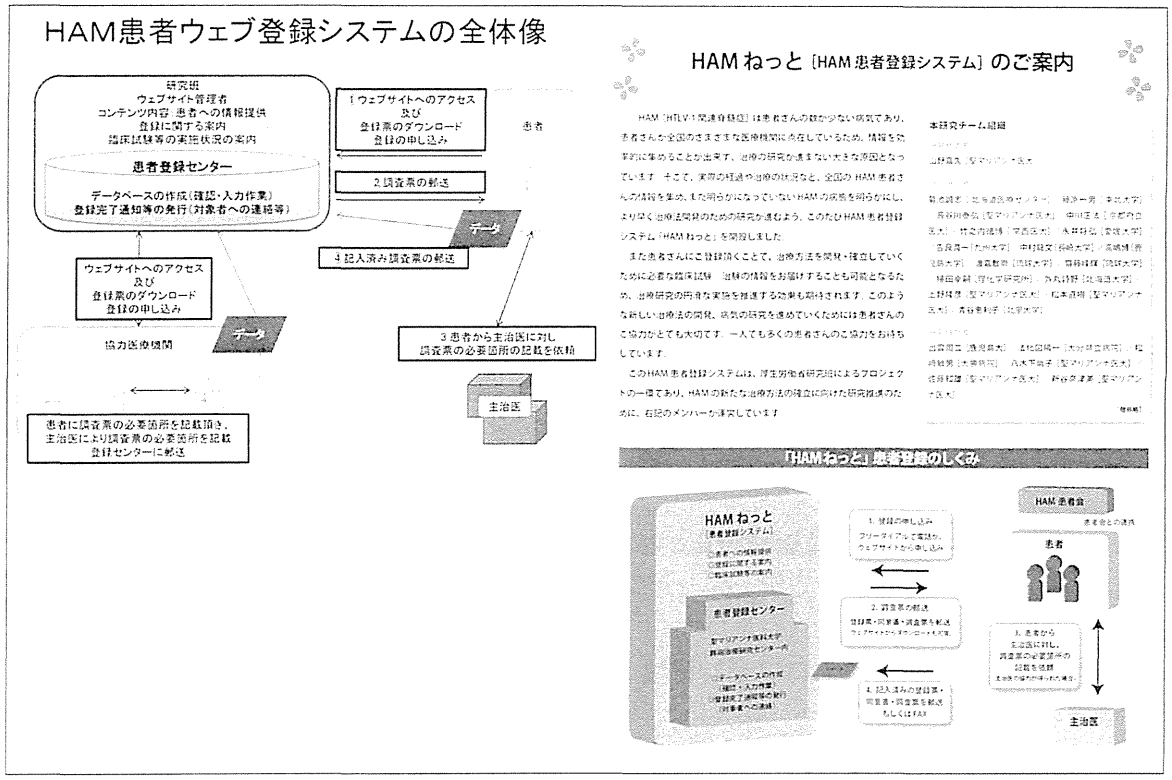

図8　HAMねっと(HAM患者登録システム)
このシステムは「HTLV-1関連脊髄症（HAM）の新規医薬品開発に関する研究」班（研究代表者聖マリアンナ医科大学　山野嘉久先生）によって運営されている.

FoxP3$^+$CD4$^+$T細胞の割合が増加し，GITRとCTLA-4の発現が有意に低下し，HTLV-1はFoxP3$^+$CD4$^+$T細胞に高頻度で感染していると報告した．制御性T細胞が抑制機能を果たす時に重要な分子であるGITRやCTLA-4が低下していたことから，HAM患者で増加しているFoxP3$^+$CD4$^+$T細胞は抑制機能が低下している可能性を指摘している[38]．HAMの脊髄では，慢性炎症が持続していると考えられるが，そのメカニズムとして，HAMの脳脊髄液中にはCXCL10/IP10レベルが高く，CXCL10結合受容体CXCR3を発現している細胞が多いことが明らかとなった．HAM患者脊髄のアストロサイトがCXCL10を主に産生しており，そのCXCL10が末梢血中単核細胞を脊髄内へ誘導している可能性が指摘されている．従って，HTLV-1感染細胞がIFN-γを産生し，IFNγがアストロサイトに作用してCXCL10を分泌させ，CXCL10がCXCR3を介して感染細胞を脊髄にさらに誘導する“positive feedback loop”がHAMにおける慢性炎症を惹起していることが示唆されている[39]．

近年，ATLに対するヒト化抗CCR4モノクローナル抗体が認可されたが，CCR4はHAMにおける感染細胞のマーカーとしても重要であり[36]，HAMに対する有効性も期待される．

R. HTLV-1対策の強化

近年，HTLV-1対策が強化され，①感染予防対策，②相談支援（カウンセリング），③医療体制

の整備，④普及啓発・情報提供，⑤研究開発の推進が掲げられた．その結果，新たな厚生労働省研究班が組織され，全国的なHAM患者登録事業（HAMねっと）がスタートした（図8）．また，ATL研究者も含めた「HTLV-1研究会・合同班会議」が組織され年々活発になっており，HAM研究は新たな時代を迎えている．

〈謝辞〉

本研究の一部は，厚生労働科学研究費補助金（エイズ研究事業）「NeuroAIDSの発症病態と治療法の開発を目指した長期フォローアップ体制の構築に関する研究（H18—エイズ—一般—009）」，同（難治性疾患克服研究事業）「重症度別治療指針作成に資するHAMの新規バイオマーカー同定と病因細胞を標的とする新規治療法の開発」班，および同「HTLV-1関連脊髄症（HAM）の新規医薬品開発に関する研究」班の助成を受けて行われた．

文献

1) Yoritaka A, Ohta K, Kishida S. Prevalence of neurological complications in Japanese patients with AIDS after the introduction of HAART. 臨床神経. 2007; 47: 491-6.
2) Spudich S, González-Scarano F. HIV-1-related central nervous system disease: current issues in pathogenesis, diagnosis, and treatment. Cold Spring Harb Perspect Med. 2012; 2: a007120.
3) Croucher A, Winston A. Neurological complications of HIV. Medicine. 2013; 41: 8; 450-5.
4) Antinori A, Arendt G, Becker JT, et al. Updated research nosology for HIV-associated neurocognitive disorders. Neurology. 2007; 69: 1789-99.
5) Gandhi NS, Moxley RT, Creighton J, et al. Comparison of scales to evaluate the progression of HIV associated neurocognitive disorder. HIV Ther. 2010; 4: 371-9.
6) Simioni S, Cavassini M, Annoni JM, et al. Cognitive dysfunction in HIV patients despite long-standing suppression of viremia. AIDS. 2010; 24: 1243-50.
7) European Treatment Guideline. http://www.europeanaidsclinicalsociety.org/
8) 三浦義治，岸田修二．HIV感染に伴う神経疾患．Brain and Nerve. 2013; 65: 275-81.
9) Schouten J, Cinque P, Gisslen M, et al. HIV-1 infection and cognitive impairment in the cART era: a review. AIDS. 2011; 25: 561-75.
10) 中川正法．HIV感染と神経合併症．Clin Neurosci. 2010; 28: 331-4.
11) Jaeger LB, Nath A. Modeling HIV-associated neurocognitive disorders in mice: new approaches in the changing face of HIV neuropathogenesis. Dis Models Mechanisms. 2012; 5: 313-22.
12) Lackner AA, Lederman MM, Rodriguez B. HIV pathogenesis-The host. Cold Spring Harb Perspect Med. 2011; a007005.
13) Xing HQ, Hayakawa H, Gelpi E, et al. Reduced expression of excitatory amino acid transporter 2 and diffuse microglial activation in the cerebral cortex in AIDS cases with or without HIV encephalitis. J Neuropathol Exp Neurol. 2009; 68: 199-209.
14) Xing HQ, Moritoyo T, Mori K, et al. Expression of proinflammatory cytokines and its relationship with virus infection in the brain of macaques inoculated with macrophage-tropic simian immunodeficiency virus. Neuropathology. 2009; 29: 13-9.
15) 岸田修二．HAART導入後の神経系AIDSとその関連疾患—真菌性髄膜炎を含めて．Neuroinfection. 2009; 14: 78-84.
16) Johnson T, Nath A. Neurological complications of immune reconstitution in HIV-infected populations. Ann N Y Acad Sci. 2010; 1184: 106-20.
17) Zaffiri L, Verma R, Struzzieri K, et al. Immune reconstitution inflammatory syndrome involving the central nervous system in a patient with HIV infection: a case report and review of literature. New Microbiologica. 2013; 36: 89-92.
18) Tan IL, Smith BR, von Geldern G, et al. HIV-associated opportunistic infections of the CNS. Lancet Neurol. 2012; 11: 605-17.
19) McArthur JC, Brew BJ, Nath A. Neurological complications of HIV infection. Lancet Neurol. 2005; 4: 543-55.
20) Funata N, Maeda Y, Koike M, et al. Neuropathology of the central nervous system in acquired immune deficiency syndrome (AIDS) in Japan.

With special reference to human immunodeficiency virus-induced encephalomyelopathies. Acta Pathol Jpn. 1991; 41: 206-11.
21) Centner CM, Bateman KJ, Heckmann JM. Manifestations of HIV infection in the peripheral nervous system. Lancet Neurol. 2013; 12: 295-309.
22) Osame M, Usuku K, Izumo S, et al. HTLV-I associated myelopathy: A new clinical entity. Lancet. 1986; 1: 1031-2.
23) Osame M, Matsumoto M, Usuku K, et al. Chronic progressive myelopathy associated with elevated antibodies to HTLV-I and adult T-cell leukemia-like cells. Ann Neurol. 1987; 21: 117-22.
24) Satake M, Yamaguchi K, Tadokoro K. Current prevalence of HTLV-1 in Japan as determined by screening of blood donors. J Med Virol. 2012; 84: 327-35.
25) 出雲周二, 松崎敏男, 久保田龍二. HAMの新しい展開. 神経内科. 2011; 75: 369-73.
26) Koga M, Takahashi T, Kawai M, et al. Neuromyelitis optica with HTLV-I infection: different from acute progressive HAM? Intern Med. 2009; 48: 1157-9.
27) 梅原藤雄. HAMの臨床的多様性. 神経内科. 2011; 75: 374-9.
28) 山野嘉久, 佐藤知雄. HTLV-1関連脊髄症(HAM)の病態・治療とバイオマーカー. 日本臨牀. 2013; 71: 870-5.
29) 武澤信夫, 奥田求己, 中川正法. HAMのリハビリテーション. 神経内科. 2011; 75: 393-401.
30) Izumo S, Ijichi T, Higuchi I, et al. Neuropathology of HTLV-I-associated myelopathy-a report of two autopsy cases. Acta Paediatr Jpn. 1992; 34: 358-64.
31) Umehara F, Izumo S, Nakagawa M, et al. Immunocytochemical analysis of the cellular infiltrate in the spinal cord lesions in HTLV-I associated myelopathy. J Neuropathol Exp Neurol. 1993; 52: 424-30.
32) Umehara F, Izumo S. Takeya M, et al. Expression of adhesion molecules and monocyte chemoattractant protein-1 (MCP-1) in the spinal cord lesions in HTLV-I-associated myelopathy. Acta Neuropathol (Berl). 1996; 91: 343-50.
33) Moritoyo T, Reinhart TA, Moritoyo H, et al. Human T-lymphotropic virus type I-associated myelopathy and tax gene expression in $CD4^+$ T lymphocytes. Ann Neurol. 1996; 40: 84-90.
34) 納 光弘, 宇宿功市郎, 梅原藤雄, 他. HAMの病態と治療. 日本内科学会雑誌. 2003; 92: 1673-82.
35) Saito M, Matsuzaki T, Satou Y, et al: In vivo expression of the HBZ gene of HTLV-1 correlates with proviral load, inflammatory markers and disease severity in HAM/TSP. Retrovirology. 2009; 6: 19.
36) Yamano Y, Araya N, Sato T, et al. Abnormally high levels of virus-infected IFN-gamma$^+$ CCR4$^+$ CD4$^+$ CD25$^+$ T cells in a retrovirus-associated neuroinflammatory disorder. PLoS One. 2009; 4: e6517.
37) Araya N, Sato T, Yagishita N, et al. Human T-lymphotropic virus type 1 (HTLV-1) and regulatory T cells in HTLV-1-associated neuroinflammatory disease. Viruses. 2011; 3: 1532-48.
38) Satou Y, Utsunomiya A, Tanabe J, et al. HTLV-1 modulates the frequency and phenotype of FoxP3$^+$CD4$^+$ T cells in virus-infected individuals. Retrovirology. 2012; 9: 46.
39) Ando H, Sato T, Tomaru U, et al. Positive feedback loop via astrocytes causes chronic inflammation in virus-associated myelopathy. Brain. 2013; 136(Pt9): 2876-87.

HTLV-1のTax発現リンパ腫細胞のウシラクトフェリンによる腫瘍増殖抑制効果

ラクトフェリン 2013

田中正和[*1)]，和田直樹[*1,2)]，橋本岩雄[*1)]・竹之内徳博[*1)]，
津田洋幸[*3)]，藤澤順一[*1)]，三輪正直[*2)]

Anti-tumor effects by bovine lactoferrin on lymphoma cells expressing HTLV-1 tax

成人T細胞性白血病(ATL)は，ヒトT細胞白血病ウイルス1型(HTLV-1)感染により引き起こされる悪性リンパ腫であるが，有効な治療法がいまだに確立されていない．

本研究において，われわれはウシラクトフェリン(bLF)をマウスに前投与したあとにHTLV-1のtax遺伝子を組み込んだ白血病細胞株を移植して，その後生じた腫瘍の増殖抑制効果が有意に認められた．脾臓のHE染色では，bLF投与群の樹状細胞が多く局在する辺縁帯の肥大が認められ，さらに蛍光免疫染色では，樹状細胞とヘルパーT細胞の活性化が確認出来た．

Masakazu Tanaka[*1)], *Naoki Wada*[*1,2)], *Iwao Hashimoto・Norihiro Takenouchi*[*1)],
Hiroyuki Tsuda[*3)], *Jun-ichi Fujisawa*[*1)], *Masanao Miwa*[*2)]

Key words：ヒトT細胞白血病ウイルス1型(HTLV-1)，腫瘍増殖抑制，樹状細胞活性化

背景と目的

ヒトT細胞白血病ウイルス1型(human T-cell leukemia virus type1, HTLV-1)は世界ではじめて発見されたヒトを宿主とするレトロウイルスで，成人T細胞性白血病(adult T-cell leukemia, ATL)発症の原因となるウイルスである[1,2]．

ATLは日本の南西地方に多発し，特異な臨床像を伴うTリンパ球の悪性腫瘍性疾患として日本で見出された[3]．感染者の大多数は無症候(HTLV-1キャリア)で，ウイルス感染してから，30～50年の潜伏期間を経たあと，生涯発症約5%の割合でATLを発症，約1%がHTLV-1関連脊髄症(HTLV-1-associated myelopathy/tropical spastic paraparesis, HAM/TSP)[4]が引き起こされる．また，その他の炎症性疾患を同時に発症することも知られている[5]．かつて主に九州・沖縄地方の風土病とまでいわれていたATLだが，近年の疫学調査ではHTLV-1キャリアが関東，近畿の大都市圏をはじめ全国に拡大していると報告されており，ウイルス排除を目指した対策が必要

*1) Department of Microbiology, Kansai Medical University 関西医科大学微生物学
*2) Bioscience, Nagahama Institute of Bio-Science and Technology 長浜バイオ大学バイオサイエンス学部
*3) Department of Molecular Toxicology, Nagoya City University Graduate School of Medical Sciences 名古屋市立大学分子毒性学分野

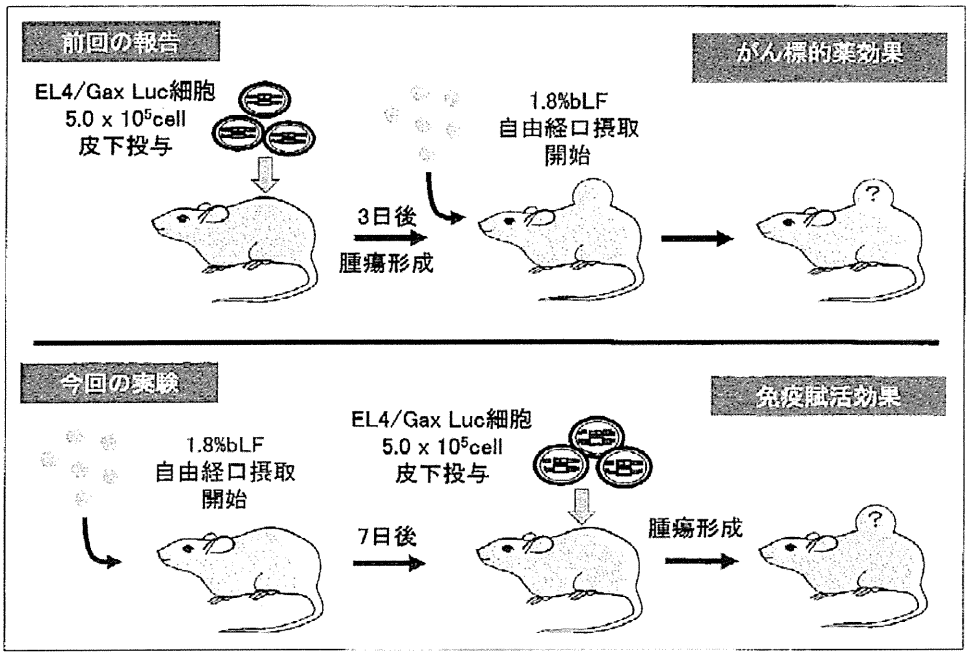

図1　HTLV-1抗原を発現する細胞(EL4/Gax細胞)をマウスへ移植したあとにウシラクトフェリン(bLF)をがん標的の効果として検討した前回の報告(上段)とウシラクトフェリン(bLF)を事前に自由経口摂取したあとにHTLV-1抗原を発現する細胞(EL4/Gax細胞)を移植し免疫賦活剤としての効果を検討した今回の報告(下段)の概略図

であるといわれている．さらに同時にHTLV-1キャリアの高齢化も懸念されており，高齢者への現行の治療方法(骨髄療法や多くの抗がん剤を用いた化学療法)では体への負担が非常に大きく，有効な治療法はいまだ確立されておらず，改善が求められているのが現状である．

筆者らは以前bLF投与が*in vitro*および*in vivo*におけるHTLV-1感染を抑制する効果が認められたことを報告し，HTLV-1の発がん遺伝子産物Taxを発現させた細胞を移植することでリンパ腫が形成されるモデルマウスを用いて，bLFがこのリンパ腫形成時において腫瘍標的薬としての抑制効果が認められることを報告した[6](図1上)．

そこで今回われわれは，Tax発現EL4細胞(EL4/Gax)を同系(B6)マウスに移植する1週間前から経口自然摂取させることで，生体内の免疫力を向上させる，すなわち免疫賦活化作用として，bLFがHTLV-1腫瘍細胞増殖を抑制することが出来るのかを調べることとした(図1下)．

材料と方法

1．ラクトフェリン(LF)

本実験で使用したLFは，森永乳業栄養科学研究所より恵与されたウシラクトフェリン(bLF)を使用した．

2．細胞株とマウスへの投与方法

MLV LTR U3領域をHTLV-1のLTRと入れ替え，Taxと蛍光蛋白質GFPとの融合蛋白質Gaxを発現するように構築した組換えレトロウイルスとルシフェラーゼ遺伝子をもつウイルスベクターをマウスTリンパ腫細胞株であるEL4細胞株へ感染させてEL4/Gax-Luc細胞として用いた[6]．

培養液はRPMI1640，10% FCS，1%ペニシリン・ストレプトマイシンを用いた．また，5×10^5 cells/50 μLに調整したEL4/Gax-Luc細胞をマウス右腹部皮下に移植投与した．ジャクソンラボラトリー(Maine，USA)より購入し自家繁殖した18週齢C57BL/6(Cg)-$Tyr^{c\text{-}2j}$/J雌マウスを実

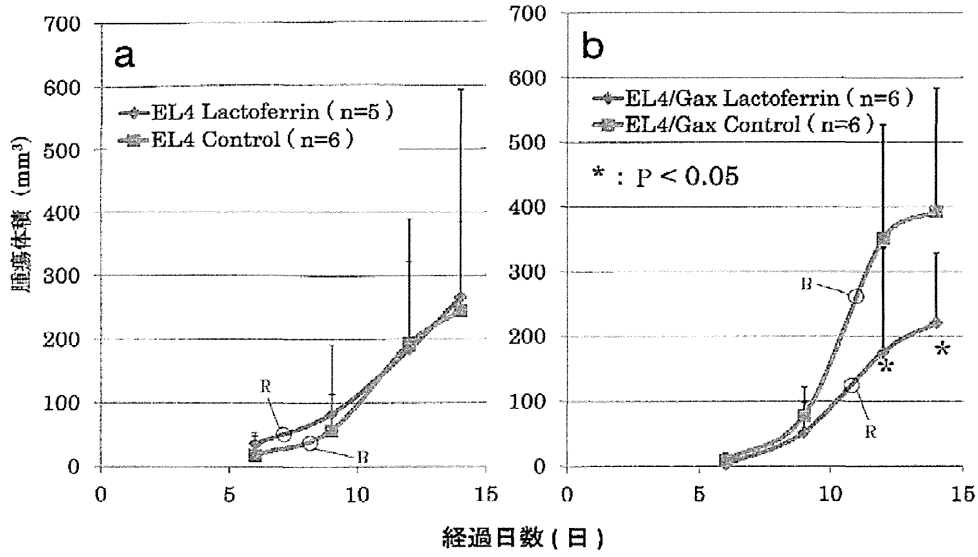

図2　触診による腫瘍体積の比較

a：EL4 細胞投与 6 日目から 14 日目までの腫瘍の体積を示した．赤実線(R)：EL4 bLF 投与群(n＝5)．青実線(B)：EL4 対照群(n＝6)

b：EL4/Gax 細胞投与 6 日目から 14 日目までの腫瘍体積を示した．赤実線(R)：EL4/Gax bLF 投与群(n＝6)．青実線(B)：EL4/Gax 対照群(n＝6)

験に用いた．

3．触診法と *in vivo* イメージング法による腫瘍体積測定

触診法についてはノギス(ミツトヨ)にて腫瘍の長径・短経および奥行を計測し，その積を腫瘍体積として評価した．また *in vivo* イメージングについては，イソフルラン(Abbott Laboratories 社製)にて麻酔を行い，ルシフェリン(Beetle Luciferin, potassium salt, Promega 社)を 3.9 mg/mL に調整して 200 μL(体重 1 kg 当たり 30 mg)を腹腔内投与した．ルシフェリン投与 20 分後，IVIS Image System(Xenogen 社)にて測定を行った．

4．パラフィン切片作成と HE 染色法

マウスから脾臓摘出後，約 3 mm 四方に切除し，15%緩衝ホルマリン溶液にて 24 時間固定を行った．その後，水道水にて水洗を行った．つづいて自動固定包埋装置(サクラファインテック・ジャパン社)にてパラフィン包埋を行い，組織のパラフィンブロックサンプルを作成した．その後，手動回転式ミクロトーム(ライカ RM2125, Leica 社)にて 4 μm に切り出し，スーパーフロストスライドガラス(MATSUNAMI 社)に貼り付けた．その後，ヘマトキシレン・エオジン染色法に準じた染色を行った．

5．凍結切片作成と蛍光免疫染色

マウスから脾臓摘出後に約 3 mm 四方になるように切り出して，ティシュー・テック(サクラファインテック・ジャパン社)に入れ，ドライアイスを入れたヘキサンに浸けて瞬間凍結した．その後，凍結切片をクリオスタットで 5～10 μm に切り出し 3-aminopropyltriethoxysilane (APS)コーティングスライドガラス(MATSUNAMI 社製)に貼り付け，30 分間風乾させた．PBS(－)で 10 分間洗浄後，2%パラホルムアルデヒド含有 PBS(－)で室温 20 分間固定を行った．PBS(－)で 5 分間×3 回洗浄後，1% BSA/PBS で 1 時間ブロッキングを行った．さらに FITC 標識抗マウス

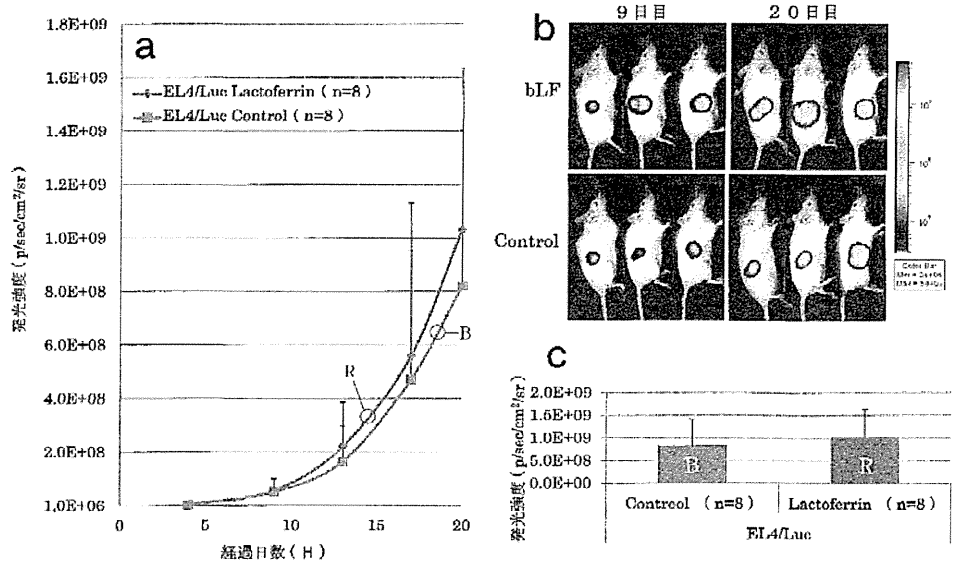

図3　*In vivo* イメージング法による腫瘍増殖比較(EL4-Luc 細胞)

a：EL4/Luc 細胞投与 4 日目から 20 日目までの bLF 投与群および対照群の発光強度を図示した．赤実線(R)：EL4-Luc bLF 投与群(n＝8)，青実線(B)：EL4-Luc 対照群(n＝8)

b：細胞投与 9 日目および 20 日目における *in vivo* イメージング写真を示した．

c：細胞投与 20 日目における発光強度を示した．赤棒(R)：EL4-Luc bLF 投与群(n＝8)，青棒(B)：EL4-Luc 対照群(n＝8)

CD4 および PE 標識抗マウス CD8(各 1% BSA/PBS で 20 倍希釈した)を 10 μL 滴下し，4℃遮光条件下で一晩抗原抗体反応を行った．その後，PBS(－)で 10 分×4 回洗浄し，95%グリセロール(Tris-HCl(pH7.4)：10 mM, 1, 4-diazabicyclo-2, 2, 2-octane[DABCO], 25 g/L, MERCK 社)にて封入した．その後，nano-zoomer(浜松フォトニクス)にて観察した．

結　果

1．マウスの体重と摂水量

本実験では，18 週齢の C57BL/6J-Tyr^{c-2J}/J(B6 albino：H-2^{b})マウスに 2% bLF 水溶液を自由摂取させた 1 週間後に EL4/Gax および EL4 細胞を皮下投与にて移植した(図 1)．移植日から全個体の体重を 3 日おきに測定したが，bLF 投与によるマウスの体重変動に有意な差は認められなかった．EL4/Gax 細胞：bLF 群(0 日目，14 日目：21.8±0.6 g，21.6±1.1 g)と対照群(0 日目，14 日目：22.0±1.1 g，21.9±0.9 g)，EL4 細胞：bLF 群(0 日目，14 日目：21.6±1.3 g，21.5±0.8 g)と対照群(0 日目，14 日目：21.6±0.4 g，21.7±0.7 g)であった．

また，摂水量においても対照群と比較して bLF 投与群では有意な差は認められなかった．EL4/Gax 細胞：bLF 群(1 回目，5 回目：4.1 mL，3.8 mL)と対照群(1 回目，5 回目：4.4 mL，4.2 mL)，EL4 細胞：bLF 群(1 回目，5 回目：3.9 mL，3.8 mL)と対照群(1 回目，5 回目：4.6 mL，4.1 mL)であった．

2．触診法による腫瘍体積の比較結果

EL4/Gax および EL4 細胞投与 5 日目から 3 日おきに測定を行い，腫瘍をノギスで長径，短経および奥行を計測し，その積を求めることで比較検討した．その結果，EL4 細胞では bLF 投与群(12 日目，14 日目：183.8±206.7 mm^3，265.8±327.5 mm^3)が対照群(12 日目，14 日目：193.0±129.8 mm^3，190.6±140.6 mm^3)で有意な差は認められなかった(図 2a)．それに対し EL4/Gax 細胞では，細胞

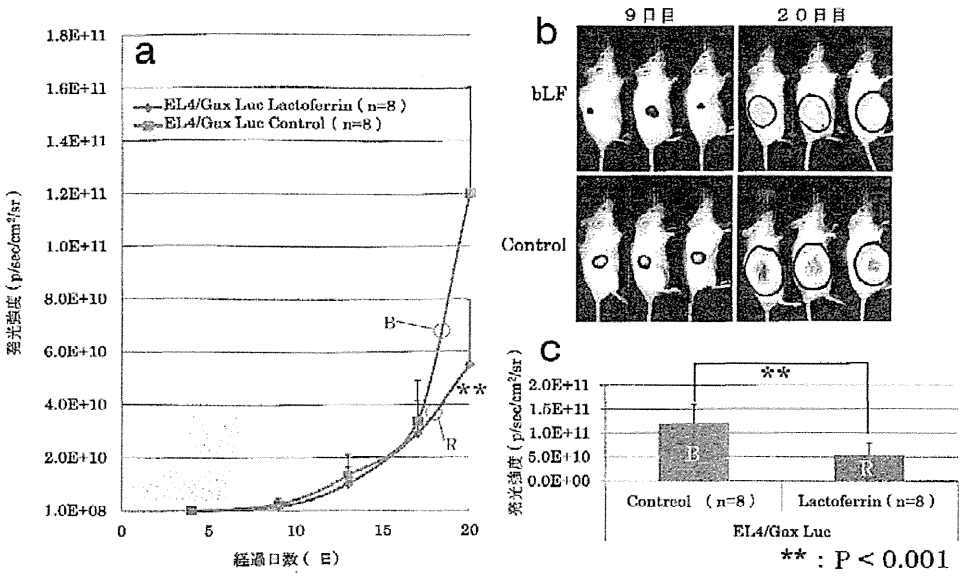

図4　*In vivo* イメージング法による腫瘍増殖比較(EL4/Gax-Luc 細胞)

a：EL4/Gax-Luc 細胞投与 4 日目から 20 日目までの bLF 投与群および対照群の発光強度を示した．赤実線(R)：EL4/Gax-Luc bLF 投与群(n－8)．青実線(B)：EL4/Gax-Luc 対照群(n＝8)

b：細胞投与 9 日目および 20 日目における *in vivo* イメージング写真をそれぞれ示した．

c：細胞投与 20 日目における発光強度を示した．赤棒(R)：EL4/Gax-Luc bLF 投与群(n＝8)．青棒(B)：EL4/Gax-Luc 対照群(n－8)

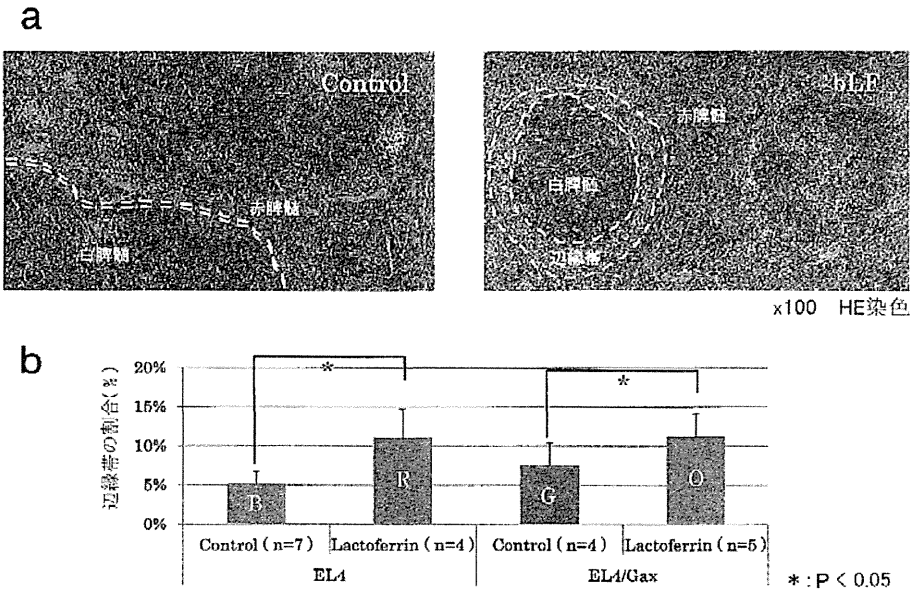

図5　ヘマトキシリン・エオジン(HE)染色法による脾臓の形態比較

a：EL4 および EL4/Gax 細胞投与マウス脾臓の HE 染色写真を示した．写真左：EL4/Gax 対照群マウスの脾臓，写真右：EL4/Gax bLF 投与マウスの脾臓．

b：脾臓全体に対する辺縁帯の占める面積の割合を示した．青棒(B)：EL4-Luc 対照群(n＝7)．赤棒(R)：EL4-Luc bLF 投与群(n＝4)，緑棒(G)：EL4/Gax-Luc 対照群(n＝5)，橙棒(O)：EL4/Gax-Luc bLF 投与群(n＝5)

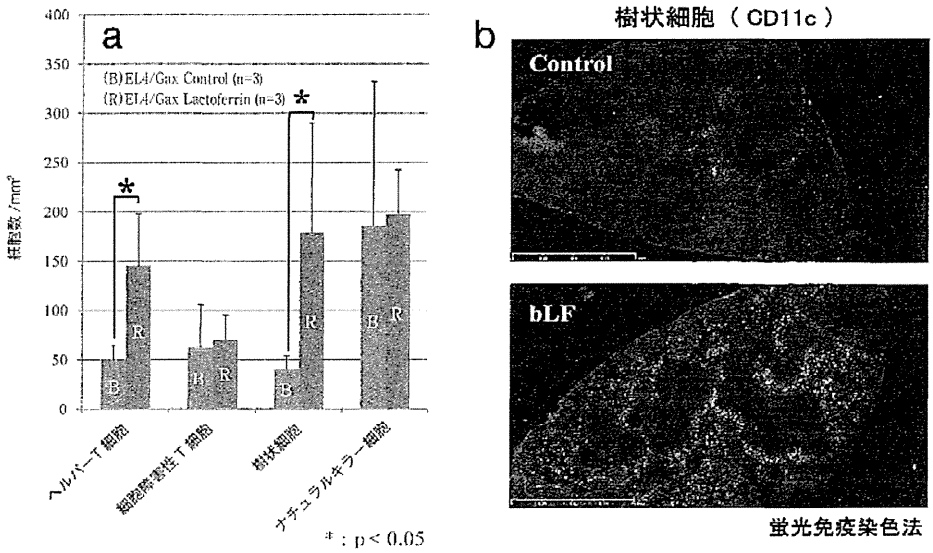

図6　蛍光免疫染色による脾臓内免疫細胞数の比較

a：マウス脾臓中での各免疫担当細胞(ヘルパーT細胞・細胞障害性T細胞・樹状細胞・ナチュラルキラー細胞)の発現数を1 mm² 当たりに換算した．青棒(B)：EL4/Gax対照群．赤棒(R)：EL4/Gax bLF群

b：樹状細胞(CD11c)での蛍光免疫染色写真．写真上：EL4/Gax 対照群脾臓．写真下：EL4/Gax bLF群脾臓

投与12日目からbLF投与群(12日目，14日目：176.0±160.8 mm³，221.1±107.7 mm³)が対照群(12日目，14日目：351.0±176.3 mm³，392.7±190.6 mm³)に比べ有意な腫瘍の増殖抑制が認められた(図2b)．

3．*In vivo* イメージング法による腫瘍増殖の比較

EL4/GaxおよびEL4細胞投与4日目から3〜5日おきに測定を行った．腫瘍の増殖度合いについては発光量の違いから判断した．EL4-Luc細胞では20日目においてbLF投与群(1.0 E+9±6.0 E+8 p/sec/cm²/sr)と対照群(8.2 E+8±5.8 E+8 p/sec/cm²/sr)で有意な差は認められなかった(図3)．それに対しEL4/Gax-Luc細胞では，細胞投与20日目においてbLF投与群(5.5 E+10±2.5 E+10 p/sec/cm²/sr)が対照群(1.2 E+11±4.0 E+10 p/sec/cm²/sr)にくらべ有意な腫瘍の増殖抑制が認められた(図4)．

4．ヘマトキシリン・エオジン(HE)染色法による形態学的な変化

免疫賦活効果の指標として，脾臓に対しHE染色を行い，bLF投与群と対照群間で形質的な違いが確認できるのかを確認した．脾臓全体に対する辺縁帯の面積の割合がEL4細胞bLF投与群(11.1％)で対照群(5.2％)，EL4/Gax細胞ではbLF投与群(11.2％)が対照群(7.5％)であり，EL4細胞，EL4/Gax細胞ともにbLF投与群が対照群比べ有意に辺縁帯の肥大化が確認できた(図5)．

5．蛍光免疫染色による脾臓内免疫細胞の数の比較

bLF投与により辺縁帯が肥大化することが確認できた．そこで辺縁帯でどのような免疫細胞が多く集積しているのかを蛍光免疫染色で調べてみた．細胞障害性T細胞およびナチュラルキラー細胞はbLF投与群(69.8±24.9，197.5±44.8)と対照群(62.75±43.2，185.7±146.7)で差は認められなかった．その一方でヘルパーT細胞および樹

状細胞はbLF投与群(145.0±52.6, 178.4±111.4)が対照群(49.3±15.1, 40.2±13.5)にくらべ有意に細胞数が増加していた(図6).

考察と今後への展望

Taxを発現するEL4/Gax細胞由来の腫瘍において, bLFによる増殖抑制効果が認められ, さらにヘルパーT細胞および樹状細胞数が有意に増加することが確認出来た. 確かにEL4/Gax細胞でbLFによりヘルパーT細胞の発現量が増加したが, 細胞性免疫を活性化するヘルパーT細胞I型(Th1)と液性免疫を活性化するヘルパーT細胞II型(Th2)のどちらが多く発現しているかは, 本実験からは特定することは出来なかった. 過去にマウスに対してbLFを配合した錠菓を摂取させると小腸上皮からインターロイキン18(IL-18)が誘導され, 細胞性免疫が高まること[7]やC型慢性肝炎患者にbLFを経口投与することで, 末梢血中においてTh2の比率が減少してTh1の比率が上昇する[8]という報告もある. したがって本実験でもTh1の比率が上昇した可能性は充分に考えられる. 本研究で用いたTax発現EL4細胞(EL4/Gax)の同系マウスに移植したこの系は, 生体内でTax特異的細胞障害性T細胞(CTL)が産生されることがすでに報告されている[9]. 筆者らはbLFにより細胞性免疫の活性化したことが, 腫瘍増殖の抑制に繋がったと考えている. またbLFの働きとして, 自然免疫系細胞であるナチュラルキラー(NK)細胞を活性化するという報告がされている[10]が, EL4細胞でのbLF投与による抑制効果は確認出来なかった. これはbLFによるNKの活性化が弱かったため腫瘍増殖の抑制までには至らなかったと考えている. 本研究ではEL4/Gax細胞マウスの脾臓でのNK細胞数は計測したが有意な差は認められず, またEL4細胞投与マウスでも同様に有意な差は認められていない.

今後の研究課題として, bLF投与によりTh1細胞が発現しているのか確かめ, 細胞性免疫を活性化させるサイトカインが放出されているのか調べる. さらにbLF投与によるTax特異的CTLの誘導能とNK細胞をはじめとする免疫担当細胞の数と活性を計測し, bLFによる腫瘍増殖抑制効果のメカニズムを解明していくことが必要である.

HTLV-1感染が原因で発症するATLは予後不良の悪性白血病であり, 有効な治療法は未だ開発されていない. ATLに対してもこれまで造血幹細胞移植による治療が試みられ, まず自家造血幹細胞移植を併用した大量化学療法に期待が寄せられたが, 移植後の高い再発率と免疫力の低下による感染症の合併のため患者の生存期間の延長は得られなかった[11]. 化学療法などの治療とともに, bLFのような副作用のない生理活性物質を併用した感染細胞の拡大阻止を行うことが, 今後のATL治療に重要であると期待している. また本研究の成果は, 現在有効な治療法がないATLの発症予防法の開発に向けた応用が期待されるだけではなく, ATL発症に至る長い潜伏期におけるHTLV-1の個体内感染動態を明らかにするうえでも重要な知見を提供するものであると考えている.

文 献

1) Poiesz BJ, Ruscetti FW, Gazdar AF, Bunn PA, Minna JD et al.: Detection and isolation of type C retrovirus particles from fresh and cultured lymphocytes of a patient with cutaneous T-cell lymphoma. Proc Natl Acad Sci USA 77: 7415-7419, 1981.
2) Reitz MS, Poiesz B, Ruscetti FW, Gallo RC: Characterization and distribution of nucleic acid sequence of a novel type C retrovirus isolated from neoplastic human T lymphocytes. Proc Natl Acad Sci USA 78: 1887-1891, 1981.
3) Uchiyama T, Yodoi J, Sagawa K, Takatsuki K, Uchino H: Adult T-cell leukemia: clinical and hematologic features of 16 cases. Blood 50(3): 481-492, 1977.
4) Hinuma Y, Nagata K, Hanaoka M, Nakai M, Matsumoto T et al.: Adult T-cell leukemia: antigen in an ATL cell line and detection of antibodies to the antigen in human sera. Proc Natl Acad Sci USA 78 (10): 6476-6480, 1981.
5) Watanabe T: HTLV-1-associated diseases. Int J Hematol 66(3): 257-278, 1997.
6) 田中正和, 鄒真美, 長谷川毅, 和田直樹・他: ウシラクトフェリンによるHTLV-1抗腫瘍効果. ラクトフェリン2011, 日本医学館, 2011, p14-20.
7) 久原徹哉: ラクトフェリンによる腸上皮からのIL-18産生誘導とその意義. 臨床免疫 34: 376-381, 2000.
8) Ishii K, Matshmaru K, Takamura N, Shinohara M,

Shinohara M et al. : Bovine lactoferrin induces serum IL-18 in patients with chronic hepatitis. J Med Soc Toho 51 : 214-221, 2004.
9) Furuta RA, Sugiura K, Kawakita S, Inada T, Ikehara S et al. : Mouse model for the equilibration interaction between the host immune system and human T-cell leukemia virus type 1 gene expression. J Virol 76 (6) : 2703-2713, 2002.
10) Kuhara T, Yamauchi K, Tamura Y, Okamura H : Oral administration of lactoferrin increases NK cell activity in mice via increased production of IL-18 and type I IFN in the small intestine. J Interferon Cytokine Res 26 : 489-499, 2006.

LYMPHOID NEOPLASIA

An animal model of adult T-cell leukemia: humanized mice with HTLV-1–specific immunity

Kenta Tezuka, Runze Xun, Mami Tei, Takaharu Ueno, Masakazu Tanaka, Norihiro Takenouchi, and Jun-ichi Fujisawa

Department of Microbiology, Kansai Medical University, Hirakata, Osaka, Japan

Key Points

- Humanized mice, IBMI-huNOG, were generated by intra–bone marrow injection of human CD133$^+$ hematopoietic stem cells.
- HTLV-1–infected IBMI-huNOG mice recapitulated distinct ATL-like symptoms as well as HTLV-1–specific adaptive immune responses.

Human T-cell leukemia virus type 1 (HTLV-1) is causally associated with adult T-cell leukemia (ATL), an aggressive T-cell malignancy with a poor prognosis. To elucidate ATL pathogenesis in vivo, a variety of animal models have been established; however, the mechanisms driving this disorder remain poorly understood due to deficiencies in each of these animal models. Here, we report a novel HTLV-1–infected humanized mouse model generated by intra–bone marrow injection of human CD133$^+$ stem cells into NOD/Shi-scid/IL-2Rγc null (NOG) mice (IBMI-huNOG mice). Upon infection, the number of CD4$^+$ human T cells in the periphery increased rapidly, and atypical lymphocytes with lobulated nuclei resembling ATL-specific flower cells were observed 4 to 5 months after infection. Proliferation was seen in both CD25$^-$ and CD25$^+$ CD4 T cells with identical proviral integration sites; however, a limited number of CD25$^+$-infected T-cell clones eventually dominated, indicating an association between clonal selection of infected T cells and expression of CD25. Additionally, HTLV-1–specific adaptive immune responses were induced in infected mice and might be involved in the control of HTLV-1–infected cells. Thus, the HTLV-1–infected IBMI-huNOG mouse model successfully recapitulated the development of ATL and may serve as an important tool for investigating in vivo mechanisms of ATL leukemogenesis and evaluating anti-ATL drug and vaccine candidates. (*Blood*. 2014;123(3):346-355)

Introduction

Human T-cell leukemia virus type 1 (HTLV-1) is a retrovirus associated with adult T-cell leukemia (ATL) and HTLV-1–associated myelopathy or tropical spastic paraparesis (HAM/TSP) in humans.[1-3] Although the majority of HTLV-1–infected individuals remain asymptomatic throughout their lives, approximately 5% of HTLV-1 carriers develop ATL or HAM/TSP following a long latency period.[4] In addition to the classic structural proteins required for retroviral replication, the HTLV-1 proviral genome encodes several accessory and regulatory proteins, including the viral transcriptional activator Tax and the HTLV-1 bZIP factor (HBZ), which are thought to be linked to HTLV-1 pathogenesis.[5,6]

ATL is an aggressive malignancy of mature CD4 T cells, characterized by frequent visceral involvement, lymphadenopathy, hypercalcemia or hypercytokinemia, and monoclonal proliferation of HTLV-1–infected tumor cells.[7] Typical ATL cells exhibit an unusual morphology with lobulated nuclei, known as "flower cells."[8] These cells are also characterized by their robust expression of interleukin (IL)-2 receptor α (CD25).[9]

To reproduce the pathogenesis of ATL, a number of mouse models have been developed, including transgenic or xenografted/humanized mice.[10-18] One such model is the Tax-transgenic mouse, which expresses Tax under the control of the Lck promoter. This model restricts Tax expression to developing thymocytes, resulting in characteristic ATL-like phenotypes.[15] Another model, the HBZ-transgenic mouse, expresses HBZ under the control of a CD4-specific promoter/enhancer/silencer. These mice develop lymphomas characterized by induction of Foxp3 in CD4 T cells, similar to leukemic cells in ATL patients.[18] These observations clearly demonstrate that the leukemogenic activity of not only Tax but also HBZ is related to the development of ATL.

In addition to transgenic mouse models, a variety of HTLV-1–infected small-animal models have been established to evaluate viral pathogenesis and elucidate the function of viral products in vivo.[19,20] These infection models have provided valuable findings regarding virus-host interactions; however, they are unable to fully recapitulate pathological conditions resembling ATL, likely due to the low efficiency of HTLV-1 infection.

Humanized mice are highly susceptible to infection with human lymphotropic viruses such as EBV, HIV-1, and HTLV-1, and have been used to recapitulate specific disorders and human immune responses.[17,21,22] Recent studies on HTLV-1 infection in humanized mouse models successfully reproduced HTLV-1–associated T-cell lymphomas[16,17]; however, these models did not accurately recreate human immune responses against HTLV-1.

Submitted June 17, 2013; accepted October 27, 2013. Prepublished online as *Blood* First Edition paper, November 6, 2013; DOI 10.1182/blood-2013-06-508861.

The online version of this article contains a data supplement.

There is an Inside *Blood* commentary on this article in this issue.

The publication costs of this article were defrayed in part by page charge payment. Therefore, and solely to indicate this fact, this article is hereby marked "advertisement" in accordance with 18 USC section 1734.

Notably, humoral immunity, along with cytotoxic T cell (CTL)-mediated cytotoxicity, is thought to play a pivotal role in controlling the proliferation or selection of HTLV-1–infected T-cell clones in vivo.[23,24] It is therefore important to develop mouse models of ATL that induce more human-like HTLV-1–specific immune responses.

In this study, we describe a novel humanized mouse model of HTLV-1 infection in the presence of specific adaptive immune responses. Our novel HTLV-1–infected humanized mice displayed distinct ATL-like symptoms, including hepatosplenomegaly, hypercytokinemia, oligoclonal proliferation of HTLV-1–infected T cells, and the appearance of flower cells. In addition, HTLV-1–specific immunity was induced and may be involved in the control of infected cells in vivo.

Materials and methods

Purification of human CD133$^+$ cells from cord blood

Cord blood samples from full-term human deliveries were obtained from the Japanese Red Cross Kinki Cord Blood Bank (Osaka, Japan) for research use due to the inadequate numbers of stem cells for human transplantation; all patients provided signed, informed consent in accordance with the Declaration of Helsinki. Mononuclear cells (MNCs) were separated using Ficoll-Conray (Lymphosepar I, IBL) density gradient centrifugation. After collecting MNCs, a CD133 MicroBead Kit (Miltenyi Biotec) was used to isolate human CD133$^+$ cells (Miltenyi Biotec) according to the manufacturer's instructions. HLA-A typing was performed using a WAKFlow HLA typing kit (WAKUNAGA) according to the manufacturer's instructions; the results are shown in supplemental Table 1 (available on the *Blood* Web site).

NOG mice

Female 6-week-old NOD/Shi-scid/IL-2Rγc null (NOG) mice[25] were purchased from the Central Institute of Experimental Animals (Kawasaki, Japan). Mice were handled under sterile conditions and were maintained in germ-free isolators. All animal experiments were approved by the Animal Care Committees of Kansai Medical University.

Generation of IBMI-huNOG

Seven-week-old NOG mice were sublethally irradiated with 250 cGy from a ^{137}Cs source (Gammacell 40 exactor, Nordion International). Within 24 hours of irradiation, each mouse was injected with 5×10^4 human CD133$^+$ cells by intra–bone marrow injection (IBMI)[26] as reported previously.[27]

HTLV-1 infection to IBMI-huNOG

The HTLV-1–infected T-cell line MT2[28] was irradiated with 10 Gy from a ^{137}Cs source irradiator. Irradiated MT2 cells (2.5×10^6) or phosphate-buffered saline were inoculated intraperitoneally into 24- to 28-week-old IBMI-huNOG mice. Mice were anesthetized and killed when the body weight decreased to <70% of their maximum weight. Peripheral blood smears were prepared using May-Grunwald Giemsa staining and examined by light microscopy. All infections were performed in a Biosafety Level P2A laboratory in accordance with the guidelines of Kansai Medical University.

Flow cytometric analysis and cell sorting

Peripheral blood cells were routinely collected every 2 weeks after infection, and after sacrificing mice, single-cell suspensions of various lymphoid tissues were prepared as described previously.[29] To stain surface markers, anti–human CD45-PerCP or APC-Cy7, CD3–fluorescein isothiocyanate (FITC) or phycoerythrin (PE)-Cy7, CD4-PE, CD8-PerCP-Cy5.5, CD19-PE, CD25-FITC, CCR4-APC antibodies were used, along with mouse immunoglobllin G1 and FITC as an isotype control (all BD Biosciences). AccuCount Ultra Rainbow Fluorescent Particles (Spherotech) were employed to determine absolute cell numbers, according to the manufacturer's protocol. Flow cytometric analysis was performed on a BD FACSCan for 3-color staining and a BD FACSCant II (BD Biosciences) for 7-color staining. The CellQuest and Diva software programs were used for data acquisition (BD Biosciences), and the collected data were analyzed by FCS express 3 (De Novo Software). Human CD4-, CD8-, and CD25-expressing T cells were sorted from splenic MNCs by FACSAria or FACSAria III (BD Biosciences).

Tetramer staining

PE-conjugated HLA-A*24:02/Tax301-309 (SFHSLHLLF) and HLA-A*24:02/HIV (RYLRDQQLL) env gp160 tetramers were purchased from MBL. Splenocytes from mock-infected or HTLV-1–infected mice were stained with each tetramer and anti–human CD3 and CD8 antibodies according to the manufacturer's protocol. Mixed lymphocyte-peptide cultures were performed to stimulate Tax-specific CTLs, as described previously.[30] Briefly, splenocytes from HTLV-1–infected mice were cultured for 13 days with 10 mg/mL Tax301-309 peptide and 50 U/mL recombinant human IL-2 (Takeda Chemical Industries). Cultured splenocytes were then analyzed by flow cytometry.

DNA isolation and quantification of proviral load

Genomic DNA was extracted from single-cell suspensions of tissue or peripheral blood using a conventional phenol extraction method. Proviral loads (PVLs) were measured by quantitative polymerase chain reaction (PCR) using a MyiQ or CFX96 real-time PCR system (Bio-Rad). The primers and probes targeting for HTLV-1 *pX* and human β-globin (HBB; as a internal control) are listed in supplemental Table 2. A plasmid containing PCR fragments for the HTLV-1 *pX* region and HBB was constructed using T-Vector pMD20 (TaKaRa) and used as the quantified standard template for real-time PCR.[31] The PVL was calculated as: [(copy number of *pX*)/(copy number of HBB / 2)] × 100.

Quantification of clonal occupancy by clone-specific PCR

Inverse long PCR (IL-PCR) was performed to amplify the genomic DNA flanked the 3′ long terminal repeat of HTLV-1 provirus according to a modified method described previously.[32] In brief, the genomic DNA was digested by *Pst*I, self-ligated by T4 ligase, and then digested by *Mlu*I. Long PCR amplification of the linearized DNA was performed using the PrimeSTAR GXL DNA polymerase (TaKaRa) according to the manufacturer's protocol. Primer sets for IL-PCR analysis are listed in supplemental Table 3. IL-PCR products were isolated from agarose gels, purified, and subjected to nested PCR. Amplified nested PCR fragments were subcloned into T-Vector pMD20 (TaKaRa) and sequenced to obtain provirus integration sites downstream of the 3′ long terminal repeat. Integration site-specific primers were designed based on the DNA sequence of the flanking region of the provirus derived from splenic DNA of 8 HTLV-1–infected mice, and are listed in supplemental Table 5. A detailed description of the clone-specific quantitative PCR procedure has been provided elsewhere.[33] The clonal occupancy of each clone was calculated as: [(copy number of integration sites)/(copy number of *pX*)] × 100.

Real-time RT-PCR to quantify *tax* and *HBZ* transcripts

Total RNA was isolated using the TRIzol reagent (Invitrogen) and complementary DNA samples were synthesized from 1 μg total RNA. Reverse-transcription PCR (RT-PCR) was performed by the use of SsoFast EvaGreen Supermix (Bio-Rad). Primers used for RT-PCR are listed in supplemental Table 4. Relative expression levels were calculated by the MyiQ system (Bio-Rad).

Titration of HTLV-1–specific antibodies

The titers of antibodies against HTLV-1 antigens in the plasma of infected mice were determined by the particle agglutination method using Serodia

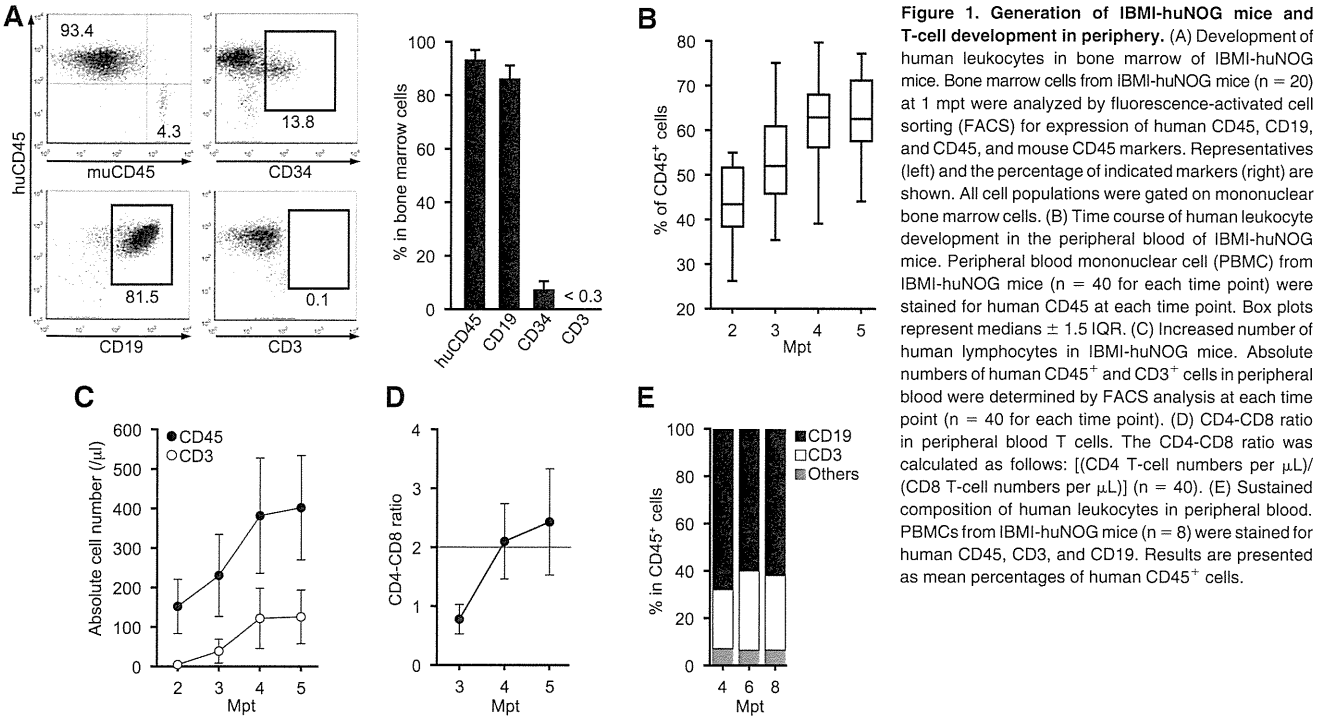

Figure 1. Generation of IBMI-huNOG mice and T-cell development in periphery. (A) Development of human leukocytes in bone marrow of IBMI-huNOG mice. Bone marrow cells from IBMI-huNOG mice (n = 20) at 1 mpt were analyzed by fluorescence-activated cell sorting (FACS) for expression of human CD45, CD19, and CD45, and mouse CD45 markers. Representatives (left) and the percentage of indicated markers (right) are shown. All cell populations were gated on mononuclear bone marrow cells. (B) Time course of human leukocyte development in the peripheral blood of IBMI-huNOG mice. Peripheral blood mononuclear cell (PBMC) from IBMI-huNOG mice (n = 40 for each time point) were stained for human CD45 at each time point. Box plots represent medians ± 1.5 IQR. (C) Increased number of human lymphocytes in IBMI-huNOG mice. Absolute numbers of human $CD45^+$ and $CD3^+$ cells in peripheral blood were determined by FACS analysis at each time point (n = 40 for each time point). (D) CD4-CD8 ratio in peripheral blood T cells. The CD4-CD8 ratio was calculated as follows: [(CD4 T-cell numbers per μL)/(CD8 T-cell numbers per μL)] (n = 40). (E) Sustained composition of human leukocytes in peripheral blood. PBMCs from IBMI-huNOG mice (n = 8) were stained for human CD45, CD3, and CD19. Results are presented as mean percentages of human $CD45^+$ cells.

HTLV-1 (Fuji Rebio).[23] To deplete human immunoglobulin M (IgM) or immunoglobulin G (IgG), streptavidin M-PVA magnetic beads (Chemagen) preincubated with biotin-conjugated goat anti–human IgM or IgG antibody (Sigma-Aldrich) were added to plasma from infected mice; a goat anti–mouse IgG antibody (Organon Teknika) was used as the negative control.

Bio-Plex cytokine assay

Plasma levels of IL-1b, IL-2, IL-4, IL-5, IL-6, IL-7, IL-8, IL-10, IL-12 (p70), IL-13, IL-17, granulocyte colony-stimulating factor (G-CSF), granulocyte macrophage colony-stimulating factor (GM-CSF), interferon-γ (IFN-γ), MCP-1, MIP-1β, and tumor necrosis factor α (TNF-α) in HTLV-1–infected and control mice were analyzed using the Bio-Plex Human Cytokine 17-Plex Panel (Bio-Rad) on a Bio-Plex 200 system according to the manufacturer's instructions.

Statistical analysis

The significance of differences was determined by Mann-Whitney *U* test, paired *t* test, or Spearman's rank-correlation coefficient (*r*); $P < .05$ was considered to indicate statistical significance.

Results

Reconstitution of human immune cells in NOG mice using IBMI

IBMI-huNOG mice were generated by IBMI of human $CD133^+$ hematopoietic stem cells into sublethally irradiated 6- to 7-week-old NOG mice. After 1 month of transplantation, human $CD45^+$ leukocytes were found to have almost completely reconstituted the bone marrow of recipient mice (Figure 1A). At this time point, the majority of the human leukocytes in bone marrow consisted of $CD19^+$ cells. A substantial number of $CD34^+$ cells were also detected, whereas human $CD3^+$ cells had not developed.

Less than half of peripheral blood cells were composed of human leukocytes even at 2 months posttransplantation (mpt). However, the number of human leukocytes increased in a time-dependent manner (Figure 1B-C). Between 3 and 4 mpt, the number of human $CD3^+$ T cells in the peripheral blood increased dramatically, as did the CD4-CD8 ratio (Figure 1D). $CD3^+$ T cells and the CD4-CD8 ratio reached stable levels by 4 to 5 mpt, suggesting that the development of human T cells was completed within this period.

Previous reports have shown that reconstituted human $CD45^+$ cells in other types of humanized mouse systems were overcome by $CD3^+$ T cells within several months of transplantation due to the reduction of B-cell development,[21,34] which may impair the integrity of host immunity. In contrast, the IBMI-huNOG mice model maintained a stable number of $CD3^+$ T cells as well as the B- to T-cell ratio in peripheral blood through at least 8 mpt (Figure 1E). Thus, the human immune system appeared to be effectively reconstituted in IBMI-huNOG mice, likely due to the enriched repopulation of long-term hematopoietic stem cells by direct injection of $CD133^+$ cells into the bone marrow cavity.[27]

Proliferation of HTLV-1–infected T cells in IBMI-huNOG mice

Human T lymphocytes fully developed in IBMI-huNOG mice within 4 to 5 mpt. These mice were then infected with HTLV-1 by intraperitoneal inoculation with 2.5×10^6 irradiated MT2 cells. The number of human $CD45^+$ leukocytes began to increase as early as 4 to 6 weeks postinoculation (wpi) and continued to increase rapidly thereafter (Figure 2A). HTLV-1 infection was also detected by 2 wpi, with the HTLV-1 PVL in peripheral blood increasing in a time-dependent manner (Figure 2B). The proportion of $CD3^+/CD45^+$ T lymphocytes was significantly enriched in HTLV-1–infected mice relative to mock-infected controls (Figure 2C), consistent with previous results.[16] Absence of residual MT2 cells used as the source of HTLV-1 was confirmed by MT2 cell-specific PCR as previously described (supplemental Figure 1).[35]

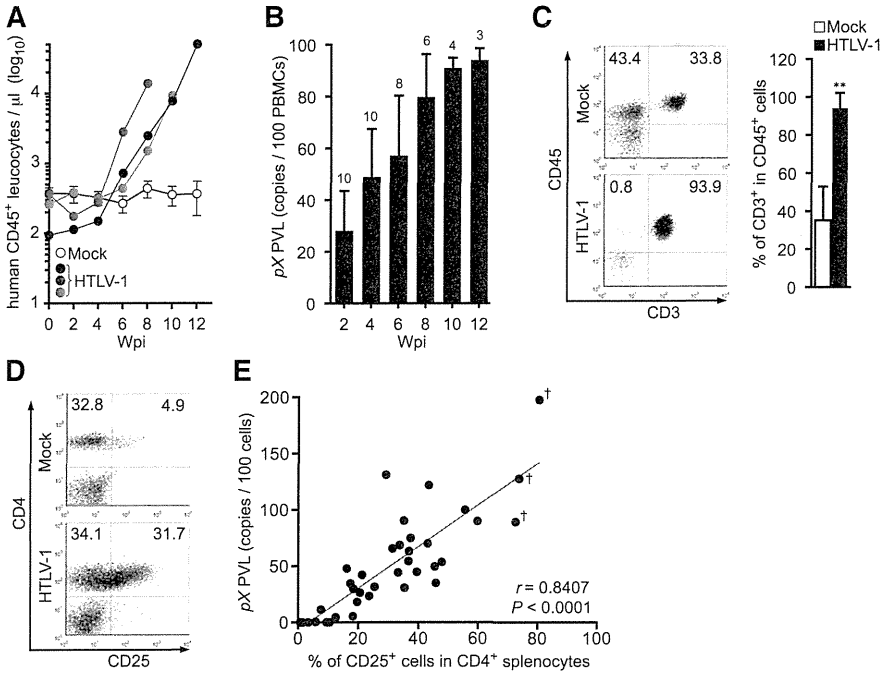

Figure 2. Kinetic analysis of HTLV-1 provirus in infected IBMI-huNOG mice. (A) Quantification of leukocyte numbers in the peripheral blood of HTLV-1–infected mice. Peripheral blood was routinely collected from mock- and HTLV-1–infected mice every 2 weeks. Human CD45$^+$ leukocytes were enumerated by FACS. Results from mock-infected mice (n = 10) are presented as mean ± standard deviation (SD), and representative results of 3 HTLV-1–infected mice are shown. (B) Quantification of HTLV-1 PVL in the peripheral blood of HTLV-1–infected mice. The PVL was determined by real-time PCR. Number at the top of each bar represents the number of analyzed HTLV-1–infected mice at each time point. (C) Expansion of CD3$^+$ T-cell populations in the peripheral blood of HTLV-1–infected mice. PBMCs from mock-infected (n = 3) and HTLV-1–infected mice (n = 18) were stained for human CD3 when sacrificed; the median value was 8 wpi. Results are presented as the average percentages ± SD of human CD45$^+$ cells. (D) Expansion of CD25$^+$ CD4 T cells in the spleen of HTLV-1–infected mice. Splenocytes were stained for human CD3, CD4, and CD25 and analyzed by FACS. Representative results from mock-infected (mouse ID: 8X20) and HTLV-1–infected (mouse ID: 8X01) mice are shown. (E) Correlation between the percentages of CD25$^+$ T cells and PVLs in the spleen. HTLV-1–infected mice (n = 37) were sacrificed to determine PVL and CD25$^+$ T-cell frequency in CD4$^+$ splenocytes. One dot represents the result of an individual HTLV-1–infected mouse. Spearman's rank-correlation coefficient (r) was adopted to identify statistically significant correlations between values. Daggers indicate that flower cells were observed in the peripheral blood of HTLV-1–infected mice.

HTLV-1–infected humanized mice showed marked expansion of CD25$^+$ CD4 T cells in the spleen relative to mock-infected controls (Figure 2D; Table 1), as is observed in peripheral blood of ATL and HAM/TSP patients.[9,36] Furthermore, PVLs in the spleen were significantly correlated with the rate of CD25$^+$ CD4 T cells (Figure 2E). These data suggest that the expanded CD25$^+$ CD4 T-cell population represents the majority of HTLV-1–infected cells in vivo.

ATL-like leukemic symptoms in HTLV-1–infected IBMI-huNOG mice

The majority of HTLV-1–infected mice exhibited splenomegaly, while apparent infiltration of infected T cells in the liver was observed in 3 infected mice with flower cells (Figure 3A; Table 1) and the weight of liver in these mice was remarkably increased (HTLV-1: 1550 ± 620 mg [n = 3]; mock: 715 ± 85 mg [n = 3]). When PVLs of several lymphoid organs were analyzed, the proportions of infected cells in the bone marrow and lymph nodes were significantly lower than those in the spleen and peripheral blood, consistent with the leukemic phenotype of infected mice (Figure 3B). This result is in striking contrast to other humanized mouse models, in which HTLV-1 infection[17] or the ectopic expression of Tax[16] preferentially induce lymphoma.

May-Grunwald Giemsa staining of peripheral blood smears from infected mice revealed the presence of large, abnormal leukemic cells with lobulated nuclei, which were morphologically identical to the flower cells observed in ATL patients (Figure 3D-E).[8] The activated phenotype of infected T cells was also evident, with clear downregulation of CD3 expression on the surface of peripheral T cells in HTLV-1–infected mice, similar to that seen in ATL cells (Figure 3C).[37]

ATL cells have been shown to secrete proinflammatory cytokines, such as IL-6, TNF-α, and GM-CSF, which stimulate activation and proliferation of infected T cells and promote development of ATL leukemogenesis.[38-40] Analysis of cytokine and chemokine levels in the plasma of HTLV-1–infected mice revealed significantly elevated levels of several proinflammatory cytokines (Figure 4). The concentration of IFNγ significantly correlated with PVL in the peripheral blood (supplemental Figure 2), suggesting Th1 immune responses induced in infected mice. Together, these results suggest that HTLV-1–infected IBMI-huNOG mice accurately recreate many of the pathological features of ATL, including hepatosplenomegaly, leukemic T-cell overgrowth with lobulated nuclei, hypercytokinemia, and downregulation of CD3 on T cells.

Oligoclonal proliferation of human T-cell clones in HTLV-1–infected IBMI-huNOG mice

To evaluate the clonal proliferation of HTLV-1–infected T cells in infected mice, we quantified cellular clonality using clone-specific real-time PCR analysis. Splenocytes were isolated from 8 infected mice sacrificed at various time points, and genomic DNA fragments

Table 1. Pathological features of mock- or HTLV-1–infected IBMI-huNOG mice

Mouse ID*	Wpi†	PVL‡	$CD3^+CD4^+$ (%)§	$CD4^+CD25^+$ (%)§	Spleen weight (mg)	Lymph node weight (mg)‖	Observations
8807	—	—	16.7	2.6	45	1	Mock infected
8X10	—	—	20.2	3.4	51	3	Mock infected
8X20	—	—	36.5	4.4	40	2	Mock infected
8401	17	65.6	53.1	31.4	195	23	
8402	11	0.1	5.3	0.7	26	1	
8403	14	0.1	10.8	3.4	35	1	
8404	17	5.4	53.4	18.3	68	2	
8405	12	11.3	30.3	7.6	59	14	
8406	5	0.1	10.5	1.5	33	3	
8407	8	4.5	69.6	12.5	166	9	
8801	25	0.1	59.6	10.4	187	7	
8803	30	0.4	38.6	5.8	55	11	
8804	23	0.1	46.6	9.5	105	5	
8805	8	70.0	57.0	43.1	233	37	Leukemia
8808	8	26.5	52.5	20.6	101	40	
8810	4	42.2	55.4	21.3	40	22	
8X01	5	44.9	65.8	39.5	208	11	
8X04	8	121.9	62.2	43.5	165	7	Leukemia
8X05	23	127.7	81.4	73.9	226	8	Leukemia, flower cells (10.6%),¶ tumor lesion
8X06	9	31.6	50.5	25.5	155	5	
8X09	5	34.6	52.2	17.4	227	9	
8X12	4	47.9	58.5	16.2	188	11	
8X14	25	68.6	51.4	33.8	145	25	Leukemia
8X16	7	90.4	78.9	35.2	200	16	Leukemia
8X17#	9	131.1	44.6	29.3	200	35	Leukemia
8X18	18	197.7	89.4	80.5	358	28	Leukemia, flower cells (19.2%),¶ tumor lesion
9Z01	10	53.6	75.8	47.9	220	12	Leukemia
9Z03	6	23.4	51.6	23.7	38	18	
9Z17	6	18.2	64.7	19.7	163	10	
9Z18	16	89.2	80.4	72.7	285	5	Leukemia, flower cells (4.2%),¶ tumor lesion
9Z19	6	35.0	65.0	45.9	207	20	
X202	12	90.0	76.6	59.9	353	13	Leukemia
X206	8	54.4	56.6	36.7	317	15	
X207**	11	100.0	62.2	55.7	358	6	Leukemia
X208	4	29.9	74.7	18.4	188	15	
X209	7	30.8	74.4	35.4	270	21	
X212	9	74.9	56.8	37.4	270	5	Leukemia
X214	10	44.3	48.0	33.3	170	6	
X216	8	63.2	66.1	36.9	271	12	Leukemia
X217	7	49.6	76.9	45.5	306	18	Leukemia

Leukemia, infected mice with atypical lymphocytes >90% of PBMCs; flower cells, atypical lymphocytes with >4 lobulated nuclei in a cell; tumor lesion, tumor formation of infiltrating infected T cells in the liver.

*The 37 infected mice listed are identical to those in Figure 2E.

†The wpi when indicated mice were sacrificed.

‡PVL is expressed as number of *pX* copies per 100 cells.

§The population of indicated marker-positive cells in $CD45^+$ splenocytes.

‖The weight value of one of the largest mesenteric lymph node in each mouse.

¶The percentage of flower cells in total lymphocytes in blood smear (presented in parentheses).

#High proportion of $CD25^+$ CD8 T cells in PBMCs.

**High proportion of DP T cells in PBMCs.

flanking the major integration sites in the HTLV-1–infected cells were amplified by IL-PCR. Amplified DNA fragments were subcloned into plasmids and sequenced to confirm proper integration (supplemental Table 5). As shown in Figure 5A, the occupancy of detected clones determined by real-time PCR was < 5% in cells harvested 5 to 8 wpi, indicating polyclonal HTLV-1 infection in these mice. In contrast, 2 mice sacrificed after prolonged infection periods (18 and 23 wpi, respectively) produced high percentages of infected clones. Interestingly, these 2 mice also showed overgrowth of $CD25^+$ CD4 T cells with flower-shaped nuclei, characteristic of ATL cells (Figure 3D-E), whereas such cells were not observed in the 6 remaining mice. These findings indicate that a limited number of HTLV-1–infected T-cell clones selectively proliferated in the spleens of infected mice, resulting in an ATL-like leukemic phenotype.[33,41]

Presence of identical infected clones in $CD25^-$ and $CD25^+$ CD4 T-cell populations

Splenocytes from infected mice were sorted into $CD25^-$ or $CD25^+$ CD4 T cells and CD8 T cells; the PVL of each population was also determined. Most of the $CD25^+$ CD4 T cells isolated from the spleens of infected mice were provirus-positive, as was a significant proportion of $CD25^-$ CD4 T cells, whereas infection of CD8 T cells was rare (Figure 5B). Interestingly, *tax* expression in HTLV-1–infected $CD25^+$ CD4 T cells was suppressed compared with that in

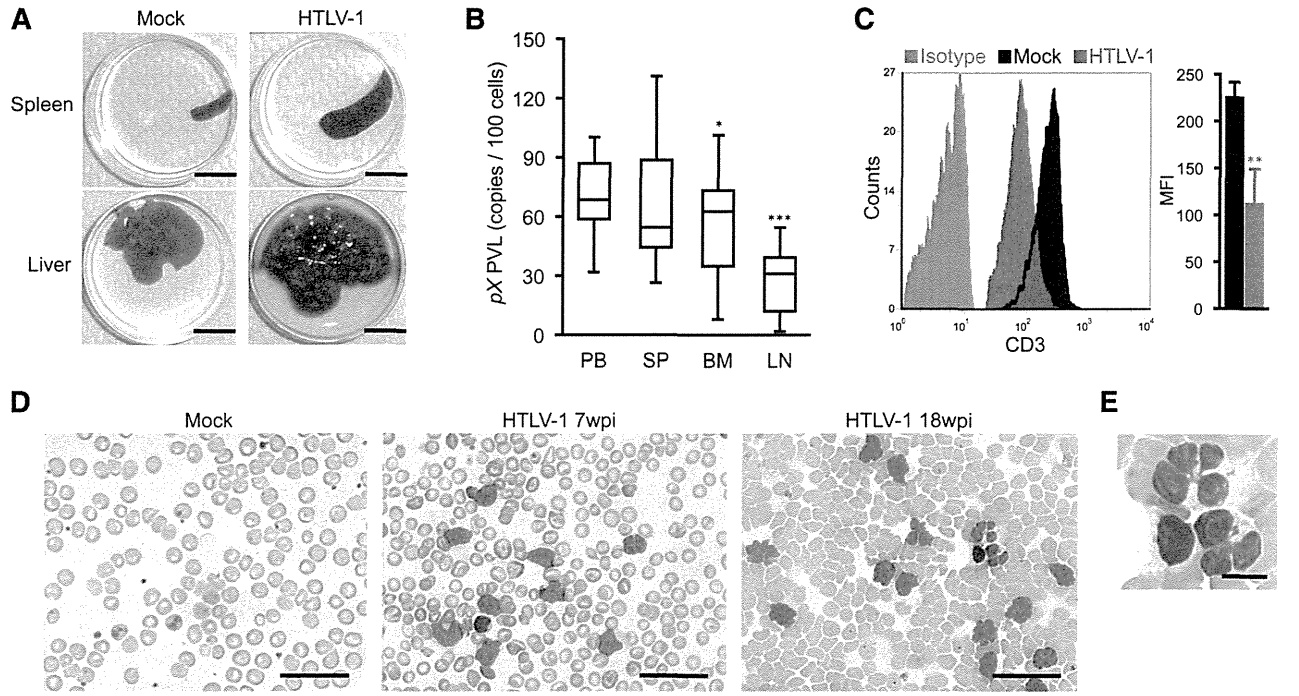

Figure 3. Splenomegaly and leukemic T-cell overgrowth in infected IBMI-huNOG mice. (A) Hepatosplenomegaly in HTLV-1–infected mice. Representative spleens and livers from mock- and HTLV-1–infected mice are shown. Scale bars in panel A represent 10 mm. (B) PVL in lymphoid organs of HTLV-1–infected mice. PVL in the peripheral blood (PB), spleen (SP), bone marrow (BM), and lymph nodes (LM) of HTLV-1–infected mice (n = 17) are shown. Box plots represent medians ± 1.5 IQR. Asterisks indicate statistical significance vs the value obtained from peripheral blood (*$P < .05$, ***$P < .001$ by paired *t* test). (C) Downregulation of CD3 on the T-cell surface. PBMCs from mock- (n = 3) and HTLV-1–infected mice (n = 18) were stained for human CD3 and analyzed by FACS. Results are presented as mean MFI ± SD of CD3 expression. (D-E) Smears of peripheral blood from HTLV-1–infected mice showing a number of leukemic cells with atypically shaped nuclei. Results from two infected mice (7 and 18 wpi, respectively) and a mock-infected mouse (at 8 mpt) are shown. Higher-magnification view of flower cells in panel D is shown in panel E. Scale bars in panels D-E represent 50 and 10 μm, respectively. Asterisks in panels B and C represent significant differences vs mock-infected mice (**$P < .01$ by Mann-Whitney *U* test).

$CD25^-$ CD4 T cells; however, higher *HBZ* expression was observed in $CD25^+$ CD4 T cells (Figure 5C).

Further clonality analysis for HTLV-1–infected $CD25^-$ and $CD25^+$ CD4 T cells isolated from the same spleen with the purity of >95% (supplemental Figure 3) revealed that the most abundant clone was the same in both T-cell populations; however, the occupancy was higher in the $CD25^+$ population (Figure 5D), indicating the preferential growth of infected clones with CD25 expression.

Induction of HTLV-1–specific adaptive immune responses in HTLV-1–infected IBMI-huNOG mice

HLA-A*24:02–restricted Tax-specific CTLs were frequently detected in ATL patients, and are known to play an important role in the control of HTLV-1–infected cells in vivo.[42-44] To investigate whether Tax-specific CTLs were induced in HTLV-1–infected mice, the IBMI-huNOG mice were generated using hematopoietic stem cells purified from the cord blood of an HLA-A*24:02 haplotype individual. HLA-A*24:02 tetramers coupled with Tax301-309 were used to detect CTLs. The cord blood HLA-A alleles used in this study are shown in supplemental Table 1. As shown in Figure 6A, Tax301-309–specific CTLs were detected in HTLV-1–infected mice at a frequency similar to that of ATL patients (0.7% ± 0.8%, n = 18),[45] whereas control tetramer CTLs specific for HIV env produced only marginal staining of CD8 T cells.

To evaluate whether functionally reactive Tax301-309–specific CTLs were present in infected mice, we cultured splenocytes from HTLV-1–infected mice in the presence of Tax peptide. Tax301-309 specific CTLs clearly proliferated following peptide stimulation; no reaction was seen in controls. Furthermore, the frequency of Tax301-309–specific CTLs in in vivo CD8 T cells was inversely correlated with the PVLs of HTLV-1–infected mice (Figure 6B). These results suggest that HTLV-1–infected mice induce functional T-cell–mediated cellular immunity against HTLV-1, which may be involved in the control of HTLV-1–infected cells in vivo.

Antibodies against HTLV-1 antigens were also detected in the plasma of infected mice as early as 2 wpi, whereas the specific antibody was not detected before infection (Figure 6C). The titer of HTLV-1–specific antibodies increased in all cases until 4 wpi, followed by a gradual decline in 67% of infected mice (4 of 6), coincident with a decrease in body weight. However, 2 of the infected mice exhibited a reactivation of antibody production at 8 wpi, suggestive of immunoglobulin class switching from IgM to IgG. In fact, HTLV-1–specific antibody titers were significantly decreased following selective depletion of human IgG, indicating the presence of functional IgG in the plasma of HTLV-1–infected mice (Figure 6D). These data clearly support the notion that the functional interaction between human T and B cells required for class switching exists in this model. Taken together, these results demonstrate that human-like adaptive immunity against HTLV-1 was established in the HTLV-1–infected IBMI-huNOG mice.

Discussion

In this study, we established a novel humanized mouse model of HTLV-1 infection. To generate humanized mice, we transplanted